Two-color cesium magneto-optical trap with $6S_{1/2}$-$6P_{3/2}$-$7S_{1/2}$ (852 nm + 1470 nm) ladder-type system

Jie Wang (王 杰)[1,2], Guang Yang (杨 光)[1,2], Jun He (何 军)[1,2,3], and Junmin Wang (王军民)[1,2,3,*]

[1]*State Key Laboratory of Quantum Optics and Quantum Optics Devices, Shanxi University, Taiyuan 030006, China*
[2]*Institute of Opto-Electronics, Shanxi University, Taiyuan 030006, China*
[3]*Collaborative Innovation Center of Extreme Optics, Shanxi University, Taiyuan 030006, China*
**Corresponding author: wwjjmm@sxu.edu.cn*

Received November 17, 2016; accepted February 17, 2017; posted online March 13, 2017

A 1470 nm + 852 nm two-color (TC) cesium (Cs) magneto-optical trap (MOT) with a $6S_{1/2}$-$6P_{3/2}$-$7S_{1/2}$ ladder-type system is proposed and experimentally investigated. To the best of our knowledge, it is the first report about the 1470 nm + 852 nm Cs TC-MOT. One of the three pairs of the 852 nm cooling and trapping beams (CTBs) in a conventional Cs MOT is replaced with a pair of the 1470 nm CTBs. Thus, the TC-MOT partially employs the optical radiation forces from photon scattering of the $6P_{3/2}$ ($F' = 5$) $-7S_{1/2}$ ($F'' = 4$) excited-state transition (1470 nm). This TC-MOT can cool and trap Cs atoms on both the red- and blue-detuning sides of the two-photon resonance. This work may have applications in cooling and trapping of atoms using inconvenient wavelengths and background-free detection of cold and trapped Cs atoms.

OCIS codes: 020.3320, 270.4180, 300.6210.
doi: 10.3788/COL201715.050203.

Laser cooling and trapping of neutral atoms in a conventional magneto-optical trap (MOT) plays an important role and has a profound impact in many fields, such as precision measurements, optical atomic clocks, quantum degenerate gases, and quantum information processing[1–3]. To date, most laser cooling schemes have used the optical radiation forces caused by photon scattering from the single-photon transition between atomic ground state and excited state. This approach has been extremely successful, leading to a range of techniques including Doppler cooling[4], polarization gradient cooling[5], and velocity-selective coherent population trapping[6]. However, there are few theoretical and experimental investigations of two-photon laser cooling in a ladder-type atomic system. Furthermore, these studies have mostly focused on the cooling of alkaline-earth-metal atoms as a second stage using the narrow $^1S_0$-$^3P_1$ inter-combination transition after the initial precooling with a strong $^1S_0$-$^1P_1$ dipole transition[7–9]. Most recently, with the development of excited-states spectroscopy[10,11], a two-color (TC) MOT based on the cesium (Cs) $6S_{1/2}$-$6P_{3/2}$-$8S_{1/2}$ (852 nm + 795 nm) ladder-type system, which partially uses the optical radiation forces from photon scattering between two excited states ($6P_{3/2}$ and $8S_{1/2}$ states), has been experimentally demonstrated[12–14]. The TC-MOT can cool and trap atoms on both the red- and blue-detuning sides of the two-photon resonance. This approach has been applied to background-free detection of trapped atoms from the related transitions driven without a laser beam with the help of narrow-bandwidth high-contrast interference filters in our previous work[13]. Also, this approach has applications in assisted cooling of certain atomic or molecular species that require lasers at inconvenient wavelengths. For instance, a laser cooling technique to cool hydrogen or anti-hydrogen atoms using the cooling transition between excited states has been proposed[15].

The primary motivation of this work is to better understand the cooling and trapping mechanism from multi-photon transitions. Figure 1(a) shows the decay channels from the Cs $8S_{1/2}$ state with a decay rate of $\Gamma' = 2\pi \times 1.52$ MHz and the $7S_{1/2}$ state with a decay rate of $\Gamma = 2\pi \times 3.30$ MHz. Compared with the Cs $6S_{1/2}$-$6P_{3/2}$-$8S_{1/2}$ TC-MOT[12–14], the Cs $6S_{1/2}$-$6P_{3/2}$-$7S_{1/2}$ TC-MOT is significantly simpler because there are fewer decay channels. Actually, the behaviors of these TC-MOTs are different in the conditions of low cooling and trapping laser intensity, which is illustrated and analyzed in the text. Consequently, it can aid in understanding the cooling and trapping mechanism in this simple ladder-type system. Another advantage of having fewer decay channels is that the

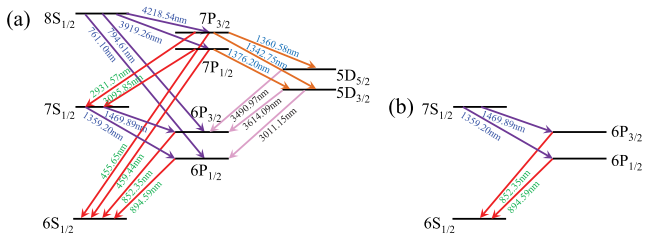

Fig. 1. Relevant energy-level and fine transitions of Cs atoms for (a) a $6S_{1/2}$-$6P_{3/2}$-$8S_{1/2}$ (852 nm + 795 nm) ladder-type system (not to scale) and for (b) a $6S_{1/2}$-$6P_{3/2}$-$7S_{1/2}$ (852 nm + 1470 nm) ladder-type system (not to scale). There are fewer decay channels from the Cs $7S_{1/2}$ state than that from the Cs $8S_{1/2}$ state, which may aid in the analysis of the cooling mechanism.

number of fluorescence wavelengths is smaller, and they are convenient to detect. Consequently, we determine the proper range of two-photon detuning and directly measure the fluorescence to diagnose the TC-MOT.

In this Letter, the Cs TC-MOT based on the Cs $6S_{1/2}$-$6P_{3/2}$-$7S_{1/2}$ (852 nm + 1470 nm) ladder-type system is proposed and experimentally investigated. To the best of our knowledge, it is the first report about the 1470 nm + 852 nm Cs TC-MOT. This scheme partially employs the optical radiation forces from photon scattering of the $6P_{3/2}$ ($F' = 5$)-$7S_{1/2}$ ($F'' = 4$) excited-state transition. One of the three pairs of the 852 nm cooling and trapping beams (CTBs) in a conventional Cs MOT is replaced with a pair of the 1470 nm CTBs. The fluorescence spectra from the $7S_{1/2}$ cascade decay are observed in the TC-MOT on both the red- and blue-detuning sides of the two-photon resonance. We measured and analyzed qualitatively the dependence of the peak fluorescence intensities on two-photon detuning, one-photon detuning, and the intensity of the CTBs. These results provide optimized experimental parameters to trap atoms.

Figure 2 shows a schematic diagram of the laser beam configuration and relevant energy-level transitions about the TC-MOT. In Fig. 1(a), the CTBs in the x–y plane comprise two pairs of counter-propagating 852 nm beams with a $1/e^2$ diameter of ~10 mm; the CTBs along the z axis (the axis of the anti-Helmholtz coils of the TC-MOT) are a pair of counter-propagating 1470 nm beams with a $1/e^2$ diameter of ~10 mm. The 852 nm repumping beams not shown in Fig. 2(a), with a $1/e^2$ diameter of ~12 mm, are sent along the $\pm y$ axis. In our experiment, the gradient of the quadrupole magnetic field generated by a pair of the anti-Helmholtz coils with current $\boldsymbol{I}$ was 1 mT/cm (10 Gauss/cm) along the z direction. The pressure of Cs vapor inside the stainless steel vacuum chamber was 1×10^{-6} Pa (7.5×10^{-9} Torr). In Fig. 2(b), the 852 nm CTBs ($\boldsymbol{\Omega}_{ge}$) that interacted with the $|g\rangle$-$|e\rangle$ transition (ω_1) have a detuning of Δ_1. The 1470 nm CTBs ($\boldsymbol{\Omega}_{ee'}$) that interacted with the $|e\rangle$-$|e'\rangle$ excited-state transition (ω_2) have a detuning of Δ_2, and the two-photon detuning is δ_2. The 852 nm repumping beams are resonant

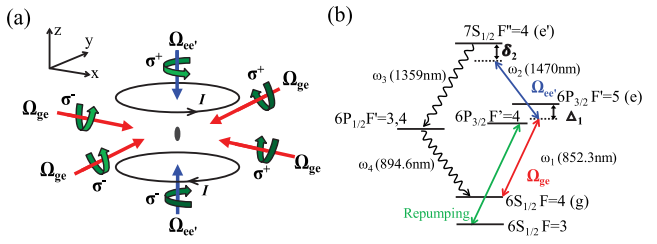

Fig. 2. (a) Schematic diagram of the laser beam configuration of the Cs TC-MOT and (b) the relevant energy levels and transitions. Four 852 nm CTBs ($\boldsymbol{\Omega}_{ge}$) couple the $|g\rangle$-$|e\rangle$ hyperfine transition, while two 1470 nm CTBs ($\boldsymbol{\Omega}_{ee'}$) couple the $|e\rangle$-$|e'\rangle$ hyperfine transition. $\boldsymbol{\sigma}^{\pm}$ are specified with respect to the positive directions of the x, y, and z axis, and $\boldsymbol{I}$ is the direct current (DC) electric current of the anti-Helmholtz coils.

with the $6S_{1/2}$ ($F = 3$)-$6P_{3/2}(F' = 4)$ transition. Decay rates for the excited states $|e\rangle$ and $|e'\rangle$ are $\Gamma = 2\pi \times 5.2$ MHz, and $\Gamma' = 2\pi \times 3.3$ MHz[16], respectively.

The cooling and trapping process in the TC-MOT arises from following two effects[12]: one is the velocity-dependent scattering force, associated with the two-photon or three-photon scattering process; another is the position-dependent restoring force, which is essential for trapping. Here, the restoring force is a result of the spatially dependent Zeeman shift of intermediate state $|e\rangle$. The restoring force has the correct sign for both positive and negative δ_2 when $\Delta_1 < 0$[12]. We mainly introduce the velocity-dependent scattering force as follows.

Two-photon scattering process. In the low-intensity regime, the dominant radiation pressure along the z axis is due to the two-photon scattering, where the first photon is absorbed from the x–y plane CTBs, and the second photon is absorbed from the z-axis CTBs. The scattering forces along the z axis can be written as $\mathbf{f}_z^{(2)} = \hbar k_{ee'} \sum_{\mathbf{i},\mathbf{j}} R_{\mathbf{i},\mathbf{j}}^{(2)} \hat{\mathbf{j}}$, where $\hat{\mathbf{i}} \in \{\hat{\mathbf{x}}, -\hat{\mathbf{x}}, \hat{\mathbf{y}}, -\hat{\mathbf{y}}\}$ is one of the four directions of the $|g\rangle$-$|e\rangle$ CTBs, and $\hat{\mathbf{j}} \in \{\hat{\mathbf{z}}, -\hat{\mathbf{z}}\}$ is one of the two directions of the $|e\rangle$-$|e'\rangle$ CTBs. For a Cs atom moving with a velocity $\mathbf{v}$, the two-photon scattering rate in the low-intensity regime can be written as[12]

$$R_{\mathbf{i},\mathbf{j}}^{(2)} = \frac{\gamma |\boldsymbol{\Omega}_{ge} \boldsymbol{\Omega}_{ee'}|^2}{16 |(\tilde{\Delta}_1 - k_{ge} \hat{\mathbf{i}} \cdot \mathbf{v})(\tilde{\delta}_2 - k_{ge} \hat{\mathbf{i}} \cdot \mathbf{v} - k_{ee'} \hat{\mathbf{j}} \cdot \mathbf{v})|^2}, \quad (1)$$

where $\boldsymbol{\Omega}_{ge}$ and $\boldsymbol{\Omega}_{ee'}$ are the Rabi frequencies of the laser-induced couplings per beam; k_{ge} and $k_{ee'}$ are the wave numbers of the $|g\rangle$-$|e\rangle$ and $|e\rangle$-$|e'\rangle$ CTBs; $\tilde{\Delta}_1 = \Delta_1 + i\Gamma/2$, and $\tilde{\delta}_2 = \delta_2 + i\gamma/2$. The Taylor expansion of Eq. (1) around $v_z = \hat{\mathbf{z}} \cdot \mathbf{v} = 0$ gives $f_z^{(2)} \approx -\alpha^{(2)} v_z$ with the two-photon damping coefficient $\alpha^{(2)} > 0$ for $\delta_2 < 0$. This is similar to the Doppler cooling process in the conventional MOT, where the Doppler effect enhances the absorption cross section for the $|e\rangle$-$|e'\rangle$ CTBs opposing the velocity $\mathbf{v}$.

Three-photon scattering process. In the moderate intensity regime of the $|g\rangle$-$|e\rangle$ CTBs, the cooling also works for positive two-photon detuning ($\delta_2 > 0$), which is opposed to the two-photon scattering cooling. This can be attributed to the three-photon and higher-order scattering processes. In the three-photon process, two-photon absorption is followed by a stimulated $|e'\rangle$-$|e\rangle$ emission. These multi-photon processes can lead to efficient cooling along the z axis in a manner similar to "Doppleron" cooling[17]. In the same way as for the two-photon case the three-photon scattering force can be written as $\mathbf{f}_z^{(3)} = \hbar k_{ee'} \sum_{\mathbf{i},\mathbf{j}} R_{\mathbf{i},\mathbf{j}}^{(3)} \hat{\mathbf{j}}$, where, for atoms moving at velocity $\mathbf{v}$, the three-photon scattering rate $R_{\mathbf{i},\mathbf{j}}^{(3)}$ is as follows[12]:

$$R_{\mathbf{i},\mathbf{j}}^{(3)} = \frac{|\boldsymbol{\Omega}_{ee'}|^2}{4|\tilde{\Delta}_1 - k_{ge} \hat{\mathbf{i}} \cdot \mathbf{v} - 2k_{ee'} \hat{\mathbf{j}} \cdot \mathbf{v}|^2} \frac{\Gamma}{\gamma} R_{\mathbf{i},\mathbf{j}}^{(2)}. \quad (2)$$

The Taylor expansion of Eq. (2) around $v_z = \hat{\mathbf{z}} \cdot \mathbf{v} = 0$ gives the three-photon damping coefficient, $\alpha^{(3)}$.

$\tilde{\Delta}_1 = \Delta_1 + i\Gamma/2$, and $\tilde{\delta}_2 = \delta_2 + i\gamma/2$. For $\Delta_1 < 0$ and $\gamma^2 = \Gamma^2 + 4\Delta_1^2$, we find $\alpha^{(3)} > 0$ for either $\delta_2 < 0$ or $\delta_2 > -\Delta_{1/2}$. Here, $\alpha^{(3)}$ involves only the three-photon process and ignores the two-photon process, light shift, and higher-order processes. The three-photon cooling effect can be understood qualitatively from the $|e\rangle$-$|e'\rangle$-$|e\rangle$ Raman process. At large $|\delta_2|$, the Doppler sensitivity along the z axis becomes independent of δ_2, but remains dependent on Δ_1. The fact that $\alpha^{(3)}$ is positive is determined by the negative Δ_1.

Usually, the absorption detection or laser-induced fluorescence after turning off the MOT can be used to estimate the number of atoms. For simplicity, here we use the fluorescence measurement to estimate the number of atoms from cold atomic cloud. The peak fluorescence intensity was directly measured by a charge-coupled device (CCD) camera to diagnose whether the MOT operates and determine the range of two-photon detuning for the MOT operation. The peak fluorescence intensities as a function of the two-photon detuning δ_2 with various single-photon detuning Δ_1 and different 852 and 1470 nm CTBs' power are shown in Fig. 3.

The significant characteristic of the TC-MOT is that fluorescence can be obtained on both the red- and blue-detuning sides of the two-photon resonance. The two-photon detuning δ_2 is controlled (from $\sim$−100 to $\sim$+100 MHz) by off-resonance TC polarization spectroscopy[18,19]. Two typical false-color fluorescence images of the cold cloud are shown as the insets of Fig. 3(a), corresponding to the data points for $\delta_2 = -36.6$ and +28.4 MHz, respectively. The sizes of the two clouds are approximately 0.8 mm (z) × 0.3 mm (x) × 0.3 mm (y) and 0.9 mm (z) × 0.2 mm (x) × 0.2 mm (y), respectively. The typical number of cold atoms is estimated to be $N \sim 5 \times 10^6$, and the corresponding atomic density of 6.9×10^{10} and 1.3×10^{11} cm^{-3}.

Figure 3(a) shows the peak fluorescence intensities of atoms trapped in the Cs TC-MOT as a function of δ_2 with various 1470 nm CTBs' power, while the 852 nm CTBs' total power is 4 × 6.10 mW, and the single-photon detuning is $\Delta_1 = -12.5$ MHz. On the red-detuning side of the two-photon resonance, as the 1470 nm CTBs' power increases, the range of δ_2 for the MOT operation broadens and is red-shifted. On the blue-detuning side, the MOT works with $\delta_2 > 12$ MHz, and the range broadens when the 1470 nm CTBs' power increases.

One point should be addressed here: the required CTBs' power for TC-MOT operation on the blue-detuning side is less than that on the red-detuning side. In detail, in the low-intensity regime, TC-MOT works only with a positive δ_2. This is opposite of that reported for a 852 nm + 795 nm Cs TC-MOT in Ref. [12], in which the required CTBs' power for TC-MOT operation on the blue-detuning side is larger. In detail, the MOT operates only for a negative δ_2 in the low-intensity regime. This is to say, for a 852 nm + 795 nm Cs TC-MOT, the three-photon process occurs only at a moderate and high intensity regime of the $|g\rangle$-$|e\rangle$ CTBs; for 852 nm + 1470 nm Cs TC-MOT, it occurs in the low-intensity regime as well.

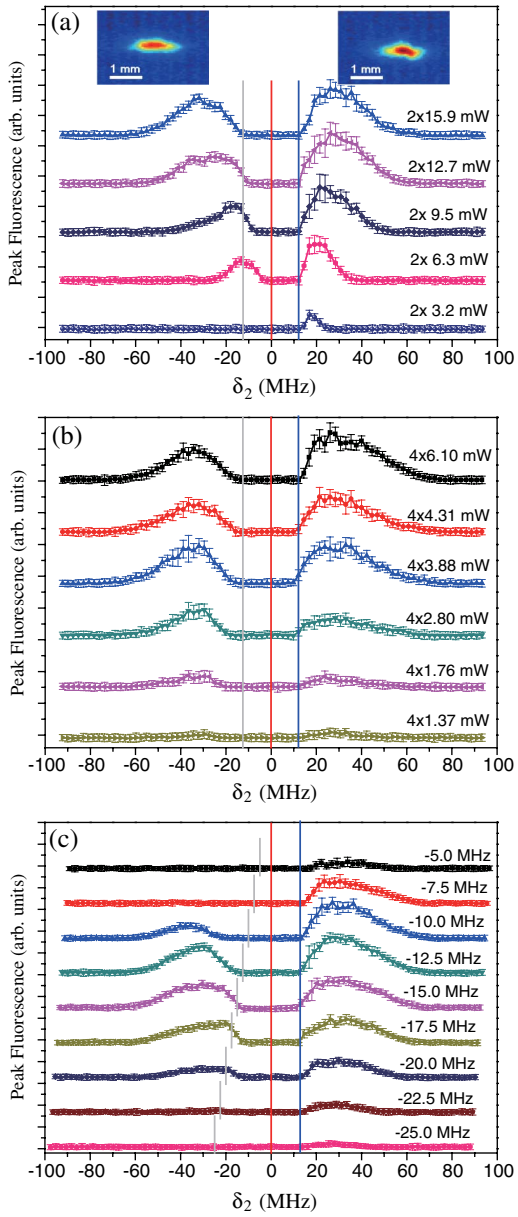

Fig. 3. The peak fluorescence intensities of Cs atoms trapped in the Cs TC-MOT as a function of the two-photon detuning δ_1, the repumping beams' total power is 2 × 2.0 mW, (a) with various 1470 nm CTBs' power, while the 852 nm CTBs' total power is 4 × 6.10 mW, and the single-photon detuning is $\Delta_1 = -12.5$ MHz. The insets are false-color fluorescence images of the cold cloud for $\delta_2 = -36.6$ and +28.4 MHz, respectively; (b) with different 852 nm CTBs' power, while the 1470 nm CTBs' total power is 2 × 20.0 mW, and $\Delta_1 = -12.5$ MHz; (c) with various Δ_1, while the 1470 nm CTBs' total power is 2 × 20.0 mW, and the 852 nm CTBs' total power is 4 × 6.10 mW. The vertical red lines in (a), (b), and (c) indicate $\delta_2 = 0$, the vertical blue lines in (a), (b), and (c) indicate $\delta_2 = +12$ MHz, and the vertical gray lines in (a) and (b) indicate $\delta_2 = -12$ MHz.

The energy levels are different in the 852 nm + 795 nm and 852 nm + 1470 nm Cs TC-MOTs, as shown in

Fig. 1. In the $6S_{1/2}$-$6P_{3/2}$-$8S_{1/2}$ TC-MOT, atoms can decay from the $8S_{1/2}$ to $6S_{1/2}$ state through cascaded $8S_{1/2}$-$7P_{3/2}(7P_{1/2})$-$6S_{1/2}$ and $8S_{1/2}$-$6P_{3/2}(6P_{1/2})$-$6S_{1/2}$ two-photon transitions, as well as the cascaded $8S_{1/2}$-$7P_{3/2}(7P_{1/2})$-$7S_{1/2}$-$6P_{3/2}(6P_{1/2})$-$6S_{1/2}$, and $8S_{1/2}$-$7P_{3/2}(7P_{1/2})$-$5D_{5/2}(5D_{3/2})$-$6P_{3/2}(6P_{1/2})$-$6S_{1/2}$ four-photon transitions. In contrast, the situation is much simpler for the $6S_{1/2}$-$6P_{3/2}$-$7S_{1/2}$ TC-MOT, where atoms can decay from the $7S_{1/2}$ to $6S_{1/2}$ state through the cascaded $7S_{1/2}$-$6P_{3/2}(6P_{1/2})$-$6S_{1/2}$ two-photon transitions. Compared with the cascade transitions in the $6S_{1/2}$-$6P_{3/2}$-$8S_{1/2}$ TC-MOT, the cascade transitions in the $6S_{1/2}$-$6P_{3/2}$-$7S_{1/2}$ TC-MOT are significantly simpler because there are fewer decay channels.

The different behaviors of the 852 nm + 1470 nm and 852 nm + 795 nm TC-MOTs are probably due to the following reasons: (1) the photon momentum at 1470 nm is less than that at 795 nm; thus, the scattering force (which is proportional to photon momentum) in the former TC-MOT is weaker than that in the latter one, so it is more difficult to cool and trap atoms in the $\delta_2 < 0$ region. In other words, more optical power is needed at the blue-detuning side for TC-MOT operation; (2) The decay channels in the former TC-MOT are much less than that in the latter one. In detail, the decay branching ratio for the $7S_{1/2}$-$6P_{3/2}$ channel is ∼65% and that for the $8S_{1/2}$-$6P_{3/2}$ channel is ∼37%; hence, the Raman process in the former TC-MOT is purer, and the three-photon scattering rate is higher in the $\delta_2 > 12$ MHz region; (3) In Eq. (2), the three-photon scattering rate is inversely proportional to $|\tilde{\Delta}_1 - k_{ge}\hat{\mathbf{i}} \cdot \mathbf{v} - 2k_{ee'}\hat{\mathbf{j}} \cdot \mathbf{v}|^2$. Consequently, it is large because $k_{ee'}$ is small along the z direction.

Figure 3(b) shows the peak fluorescence intensities of atoms trapped in the Cs TC-MOT as a function of δ_2 with various 852 nm CTBs' power, while the 1470 nm CTBs' total power is 2×20.0 mW, and the single-photon detuning is $\Delta_1 = -12.5$ MHz. As the 852 nm CTBs' power increases, the range of δ_2 for TC-MOT operation on both the red- and blue-detuning sides does not change much (neither shifts nor broadens) because of the force balance along the z direction. The 852 nm CTBs are orthogonal to the 1470 nm CTBs; as a result, when the 852 nm CTBs' power increases, the number of atoms increases, but the force balance along the z direction does not break.

Figure 3(c) shows the peak fluorescence intensities of atoms trapped in the Cs TC-MOT as a function of δ_2 with various single-photon detunings Δ_1, while the 1470 nm CTBs' total power is 2×20.0 mW, and the 852 nm CTBs' total power is 4×6.1 mW. With a change in the single-photon detuning Δ_1, the peak fluorescence intensity has an optimized value at $\Delta_1 = -12.5$ MHz. Larger or smaller than this value, the peak fluorescence intensity decreases. Note that the single-photon detuning Δ_1 seems not to shift the range of δ_2 for TC-MOT operation because the 852 and 1470 nm CTBs are perpendicular. The gray lines representing $\delta_2 = \Delta_1$ in each curve provide the most direct impression for why we consider the two-photon detuning δ_2 instead of Δ_2.

In conclusion, a novel (852 nm + 1470 nm) Cs TC-MOT, in which the optical radiation forces from photon scattering of the Cs $6P_{3/2}$-$7S_{1/2}$ excited-state transition in a Cs $6S_{1/2}$-$6P_{3/2}$-$7S_{1/2}$ ladder-type system are partially employed, is proposed and experimentally investigated. The fluorescence spectra from the $7S_{1/2}$ cascade decay are observed in the Cs TC-MOT on both the red- and blue-detuning sides of the two-photon resonance. We measure and analyze qualitatively the dependence of peak fluorescence intensities on the two-photon detuning, the one-photon detuning, and the intensity of 852 nm and 1470 nm CTBs. The behaviors of peak fluorescence intensity on the two-photon detuning with increasing $|g\rangle$-$|e\rangle$ CTBs are different from that for a 852 nm + 795 nm TC-MOT. This indicates that the three-photon process not only occurs in the moderate and high intensities regime, but also in the low intensity regime of the $|g\rangle$-$|e\rangle$ CTBs. These results not only provide optimized experimental parameters to trap atoms, but also provide helpful evidence to deeply investigate the mechanism of cooling and trapping atoms in a TC-MOT. The experiment demonstrated in this work might have wide applications, such as background-free detection of trapped atoms and laser cooling of certain atomic species that require cooling lasers at inconvenient wavelengths.

This work was supported by the National Natural Science Foundation of China under Grant Nos. 61475091, 11274213, and 61227902.

References

1. W. D. Phillips, Rev. Mod. Phys. **70**, 721 (1998).
2. H. J. Metcalf and P. van der Straten, *Laser Cooling and Trapping* (Springer-Verlag, 1999).
3. E. L. Raab, M. Prentiss, A. Cable, S. Chu, and D. E. Pritchard, Phys. Rev. Lett. **59**, 2631 (1987).
4. S. Chu, L. Hollberg, J. E. Bjorkholm, A. Cable, and A. Ashkin, Phys. Rev. Lett. **55**, 48 (1985).
5. J. Dalibard and C. Cohen-Tannoudji, J. Opt. Soc. Am. B **6**, 2023 (1989).
6. J. Hack, L. Liu, M. Olshanii, and H. Metcalf, Phys. Rev. A **62**, 013405 (2000).
7. E. A. Curtis, C. W. Oates, and L. Hollberg, Phys. Rev. A **64**, 031403 (R) (2001).
8. N. Malossi, S. Damkjær, P. L. Hansen, L. B. Jacobsen, L. Kindt, S. Sauge, J. W. Thomsen, F. C. Cruz, M. Allegrini, and E. Arimondo, Phys. Rev. A **72**, 051403(R) (2005).
9. T. E. Mehlstäubler, K. Moldenhauer, M. Riedmann, N. Rehbein, J. Friebe, E. M. Rasel, and W. Ertmer, Phys. Rev. A **77**, 021402(R) (2008).
10. J. G. Banacloche, Y. Q. Li, S. Z. Jin, and M. Xiao, Phys. Rev. A **51**, 576 (1995).
11. B. D. Yang, J. Y. Zhao, Q. B. Liang, J. F. Yang, J. He, T. C. Zhang, and J. M. Wang, Acta Sin. Quantum Opt. **15**, 180 (2009).
12. S. Wu, T. Plisson, R. C. Brown, W. D. Phillips, and J. V. Porto, Phys. Rev. Lett. **103**, 173003 (2009).
13. B. D. Yang, Q. B. Liang, J. He, and J. M. Wang, Opt. Express **20**, 11944 (2012).
14. B. D. Yang, J. Wang, and J. M. Wang, Chin. Opt. Lett. **14**, 040201 (2016).

15. S. Wu, R. C. Brown, W. D. Phillips, and J. V. Porto, Phys. Rev. Lett. **106**, 213001 (2011).
16. C. E. Theodosiou, Phys. Rev. A **30**, 2881 (1984).
17. J. J. Tollett, J. Chen, J. G. Story, N. W. M. Ritchie, C. C. Bradley, and R. G. Hulet, Phys. Rev. Lett. **65**, 559 (1990).
18. B. D. Yang, J. Wang, H. F. Liu, J. He, and J. M. Wang, Opt. Commun. **319**, 174 (2014).
19. H. F. Liu, J. Wang, G. Yang, B. D. Yang, J. He, and J. M. Wang, Chin. J. Lasers **41**, 0715004 (2014).